catalysts

MDPI

Article

Structure and Photocatalytic Activity of $PdCrO_x$ Cocatalyst on $SrTiO_3$ for Overall Water Splitting

Tomoki Kanazawa [1,2], Shunsuke Nozawa [3], Daling Lu [4] and Kazuhiko Maeda [1,*]

1 Department of Chemistry, School of Science, Tokyo Institute of Technology, 2-12-1-NE-2 Ookayama, Meguro-ku, Tokyo 152-8550, Japan; kanazawa.t.ad@m.titech.ac.jp
2 Japan Society for the Promotion of Science, Kojimachi Business Center Building, 5-3-1 Kojimachi, Chiyoda-ku, Tokyo 102-0083, Japan
3 Institute of Materials Structure Science, High Energy Accelerator Research Organization, 1-1 Oho, Tsukuba, Ibaraki 305-0801, Japan; noz@post.kek.jp
4 Suzukakedai Materials Analysis Division, Technical Department, Tokyo Institute of Technology 4259 Nagatsuta-cho, Midori-ku, Yokohama 226-8503, Japan; lu.d.aa@m.titech.ac.jp
* Correspondence: maedak@chem.titech.ac.jp; Tel.: +81-3-5734-2239

Received: 10 December 2018; Accepted: 3 January 2019; Published: 8 January 2019

Abstract: The mechanism of $PdCrO_x$ multi-component cocatalyst formation on $SrTiO_3$ was investigated using transmission electron microscopy, X-ray absorption fine structure spectroscopy and X-ray photoelectron spectroscopy. The $PdCrO_x/SrTiO_3$ samples were synthesized by a photodeposition method under UV light irradiation ($\lambda > 300$ nm) for various time periods (0–5 h). The fine structure and valence state of the Pd species of $PdCrO_x$ nanoparticles were varied from Pd oxide to a mixture of metallic Pd and oxidized Pd species with an increase in the irradiation time. The overall water-splitting activity of $PdCrO_x$ was strongly dependent on the photoirradiation time during deposition. Although longer photoirradiation time during preparation did not influence the H_2 evolution activity of $PdCrO_x/SrTiO_3$ from aqueous methanol solution, it was effective in suppressing the O_2 photoreduction activity, which is one of the backward reactions during overall water splitting.

Keywords: semiconductor photocatalyst; water splitting; cocatalyst

1. Introduction

Photocatalytic decomposition of H_2O into H_2 and O_2, using a semiconductor powder, is one of the target reactions of artificial photosynthesis in producing a clean energy source [1–4]. Many strategies have been proposed to improve the efficiency of this reaction, such as doping [5], morphological modification [6], application of visible-light-absorbing materials [7–10], cocatalyst loading [11–17] and surface protection [18,19]. With respect to surface modification, the loading of metal or metal-oxide nanoparticles, which are referred to as cocatalysts, onto the surface of a semiconductor photocatalyst has been widely employed to enhance the activity toward photocatalytic water splitting. The cocatalyst nanoparticle reduces the activation energy for reduction/oxidation reactions and suppresses charge recombination of electron and hole pairs in a semiconductor, thereby enhancing the activity.

Several cocatalysts that consist of more than two metal species have recently been reported for water splitting, and some of them have been more efficient than their single component counterparts [9–14]. Among these multi-component cocatalysts, mixed oxides of Cr and a paired transition metal have been well studied for overall water splitting. The metal-Cr mixed compounds were reported as promoters for not only the hydrogen evolution reaction (HER) but also the oxygen evolution reaction (OER). Whereas $RhCrO_x$ was reported to work as a HER cocatalyst on the surface

of various semiconductor photocatalysts [14,15], $FeCrO_x$ was recently reported to function as an OER cocatalyst on $SrTiO_3$ [17]. Therefore, metal-Cr mixed compounds are considered to be promising cocatalyst materials for water splitting.

Our group recently reported $PdCrO_x$ nanoparticles as a HER cocatalyst [16]. However, it was difficult to synthesize an active $PdCrO_x$ cocatalyst using a conventional impregnation method, and thus required a photochemical method instead (see Scheme 1). The $PdCrO_x$/semiconductor photocatalyst system is interesting from a synthetic inorganic chemistry and functional materials chemistry perspective. However, compared to a similar mixed oxide cocatalyst such as $RhCrO_x$, the structural characterization of photochemically-synthesized $PdCrO_x$ has yet to be completed, and thus the impact of the preparation conditions on the formation of $PdCrO_x$ remains unknown.

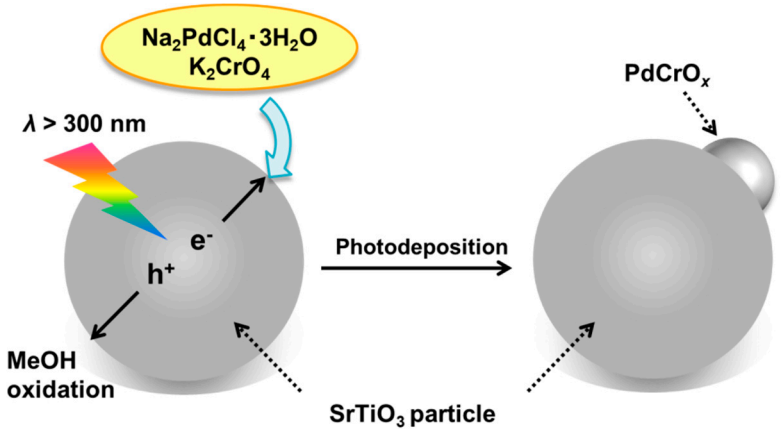

Scheme 1. Photochemical preparation of $PdCrO_x$ nanoparticles on the surface of $SrTiO_3$.

In this work, the structure of $PdCrO_x$ formed on the surface of $SrTiO_3$ with various irradiation times was characterized using high resolution transmission electron microscopy (HR-TEM), extended X-ray absorption fine structure spectroscopy (EXAFS), X-ray absorption near edge structure (XANES) and X-ray photoelectron spectroscopy (XPS).

2. Results and Discussion

2.1. Deposition of $PdCrO_x$ Nanoparticles

Figure 1 shows a typical time course for H_2 evolution observed during the photodeposition of $PdCrO_x$. After an induction period (ca. 1 h), stable H_2 evolution (ca. 63.3 μmol h^{-1}) was observed. The induction period between 0–1 h suggests that $PdCrO_x$ cocatalyst deposition was accomplished within 1 h. In the absence of the Pd and Cr sources, H_2 production was observed at a moderate rate (0.2 μmol h^{-1}). The amount of Cr deposited in the product ($PdCrO_x/SrTiO_3$) was quantified by monitoring the concentration of the Pd and Cr sources in the solution using UV-visible absorption spectroscopy. Figure 2 shows the amount of Cr deposited on $SrTiO_3$ as a function of the photoirradiation time. It is noted that all of the Pd precursor added (0.5 wt% Pd) underwent inclusion on the surface of $SrTiO_3$, regardless of the photoirradiation time. Therefore, the amount of Pd in deposited $PdCrO_x/SrTiO_3$ was identical. The amount of deposited Cr was increased with the irradiation time. Even without photoirradiation, 0.2 wt% portion of Cr disappeared from the solution phase, which suggests that the Cr species is adsorbed onto the surface of $SrTiO_3$. After 1–5 h irradiation, the amount of loaded Cr reached almost a constant value of 0.7–0.8 wt%, which indicated that Cr had been photodeposited.

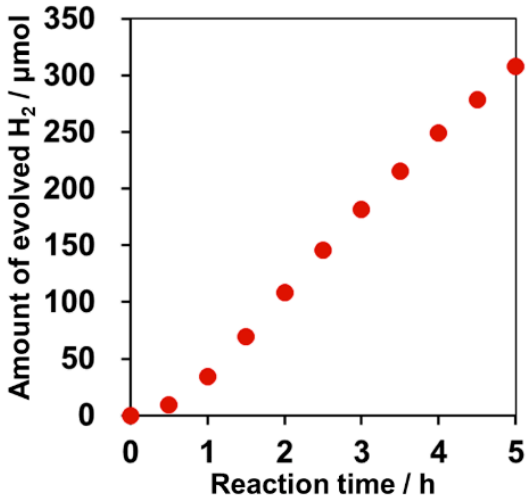

Figure 1. Time course of H_2 evolution during the photodeposition of $PdCrO_x$ nanoparticles. Reaction conditions: Catalyst, 200 mg; 10 vol% aqueous methanol solution, 100 mL; metal precursors, Pd 0.5 wt%, Cr 1.0 wt%; light source, 300 W xenon lamp (λ > 300 nm).

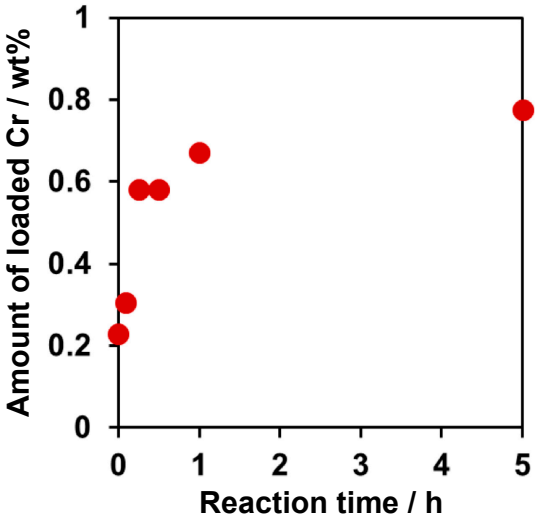

Figure 2. Amount of Cr contained in $PdCrO_x/SrTiO_3$ at various photodeposition times.

Figure 3 shows TEM images of the deposited $PdCrO_x$ nanoparticles. These observations indicated that the deposited $PdCrO_x$ nanoparticles are not only core/shell type particles (core: Metallic Pd, shell: Cr_2O_3) but also aggregates and isolated metallic Pd nanoparticles. The ratio of the deposited Pd and Cr was also different in each particle. In general, the photodeposition rate of metal nanoparticles (in other words, the rate of photoreduction of metal ions) on the semiconductor surface depends on the surface property of the semiconductor (e.g., crystal faces), as reported by Ohno et al. [20]. Because $SrTiO_3$ particles used in this work have featureless morphology, the precise control of the Pd^0 photodeposition would be difficult, leading to the compositional deviation in the Pd/Cr ratio. Metallic and oxidized Pd species were loaded on $SrTiO_3$, as evidenced by XPS measurements (discussed later). The lattice fringe attributable to metallic Pd was observed in the 5 h sample (see 5 h (1)). Therefore, the central part of the nanoparticle consisted of metallic Pd. However, the location of the oxidized Pd species in the TEM images could not be detected.

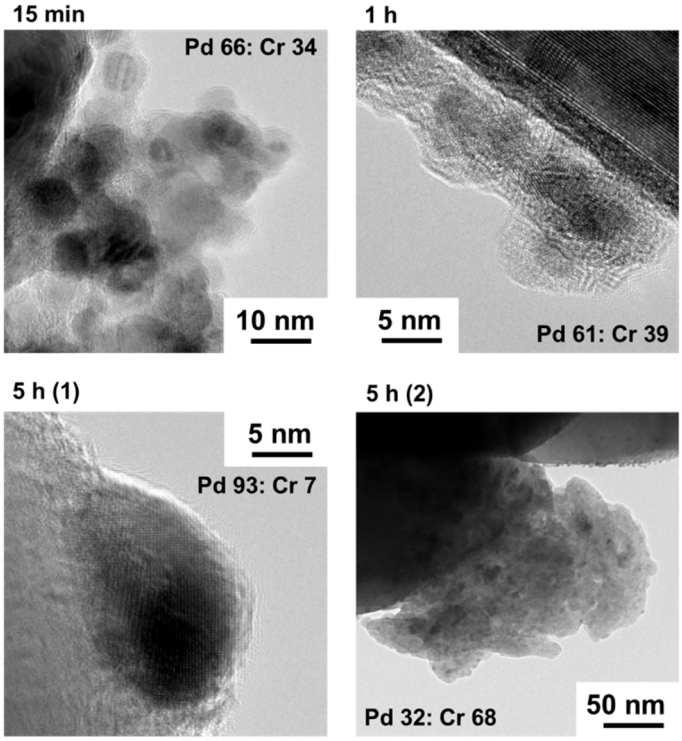

Figure 3. Transmission electron microscopy (TEM) images and Pd/Cr weight ratios of $PdCrO_x/SrTiO_3$ prepared for various time periods (15 min, 1 and 5 h). The weight ratio was calculated from energy dispersive X-ray spectroscopy (EDX) measurements.

2.2. XANES

Figure 4 shows Pd K-edge XANES spectra of $PdCrO_x/SrTiO_3$ prepared for various time periods (0–5 h). Data for Pd foil, PdO, and $Pd/SrTiO_3$ (prepared without Cr) are also shown for comparison. The spectral shapes for Pd foil and $Pd/SrTiO_3$ were very similar. Compared to metallic Pd (Pd foil and $Pd/SrTiO_3$), the absorption edges of $PdCrO_x/SrTiO_3$ were varied with respect to the irradiation time (Figure 4A). The Pd K-edge positions are located at higher energies, which indicates that their electronic density is lower than metallic Pd. Figure 4B shows an enlarged view that shows that the K-edge positions are shifted to higher energies in the following order: Pd foil ≈ Pd/STO < 15 min < 5 h ≈ 1 h ≈ 30 min < 0 h < PdO. The K-edge of the 0 h sample was located at the highest energy position among all the samples examined. The K-edge position was shifted to the lower energy side with an increase of the irradiation time to 15 min, which indicates that the adsorbed Pd precursor on $SrTiO_3$ was reduced by photoexcited electrons supplied from $SrTiO_3$ within 15 min. After 15 min, the K-edge position was shifted slightly to the higher energy side, which indicates that the electron density of the $PdCrO_x$ nanoparticles is slightly decreased after 15 min, i.e., the Pd species were oxidized. These results indicate that the electronic state of the Pd species in the $PdCrO_x$ nanoparticles is dependent on the photoirradiation time.

Cr K-edge XANES spectra of $PdCrO_x/SrTiO_3$ were also investigated, and the results are shown in Figure S1. In contrast to the Pd K-edge spectra, the Cr K-edge positions were similar, regardless of the photoirradiation time. Therefore, it is concluded that the electronic state of only Pd showed a significant change during photoirradiation.

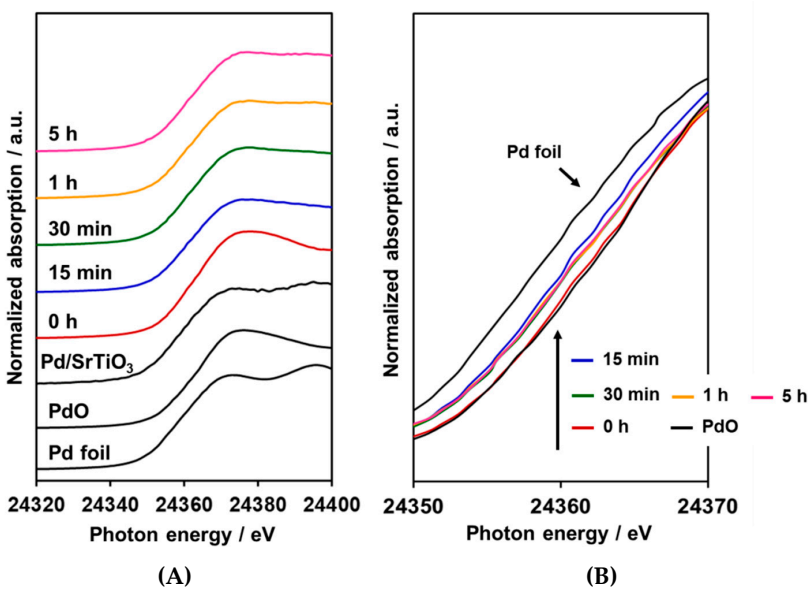

Figure 4. The Pd K-edge XANES spectra of $PdCrO_x$ nanoparticles (0–5 h) on $SrTiO_3$: (**A**) Wide view, and (**B**) narrow view. The XANES spectra of Pd foil, PdO and $Pd/SrTiO_3$ as references. The order of the K-edge positions is: (Low) < Pd foil ≈ Pd/STO < 15 min < 5 h ≈ 1 h ≈ 30 min < 0 h < PdO < (high).

2.3. EXAFS

Figure 5 shows the Fourier transforms of k^3-weighted Pd K-edge EXAFS spectra. The peak of Pd foil at 2.5 Å is assigned to Pd–Pd bonding, and the peak of PdO at 1.5 Å is assigned to Pd–O. The 0 h sample showed a peak at 1.5 Å, which indicates the presence of Pd–O bonding. In the cases of the 0–5 h samples, the intensity of Pd–O bonding became relatively weak with an increase in the photoirradiation time. On the other hand, the intensity of the Pd–Pd bonding peak was increased. Finally, the 5 h sample showed peaks for both Pd–O and Pd–Pd, which indicates that the Pd species in $PdCrO_x/SrTiO_3$ transforms from an oxide-like state to a mixture of Pd^0 and Pd oxide as photoirradiation progressed. This trend does not contradict the observation in the XANES analysis (Figure 4). Therefore, it is concluded that the Pd species is reduced from oxide to the metallic state, although not completely, during the photoirradiation process. Similar to the Cr K-edge XANES results, no noticeable change could be identified in the fine structure of Cr (Figure S1).

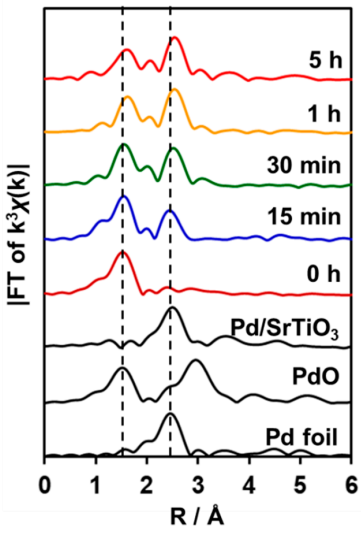

Figure 5. Fourier transforms of k^3-weighted Pd K-edge EXAFS spectra for $PdCrO_x/SrTiO_3$ prepared for various time periods (0–5 h). Data for Pd foil, PdO and $Pd/SrTiO_3$ are shown as references.

2.4. XPS

Figure 6 shows XPS Pd 3d spectra for the $PdCrO_x/SrTiO_3$ samples. All of the Pd 3d peaks can be deconvoluted into two peaks with binding energies of 337.1 and 335.2 eV, which are assigned to oxidized and metallic Pd species, respectively, although the binding energies are slightly different from those in the references (PdO: 336.5 eV; metallic Pd in $Pd/SrTiO_3$: 334.8 eV) [21]. The intensity ratio of the 335.2 eV peak becomes stronger relative to the 337.1 eV peak with an increase in the photoirradiation time, which is consistent with the trend observed in the EXAFS spectra (Figure 5). The details of the surface electronic states of $PdCrO_x$ were previously investigated using XPS [16]. The XPS Pd 3d peak position of Pd species co-existing with Cr^{3+} was thereby determined to be higher than that of bulk PdO(II). In addition, the Pd 3d peak position and structure of $PdCrO_x$ was different from the PdO(II) single oxide, and the surface absorbed Pd precursor. Therefore, the 337.1 eV peak is not a single Pd oxide or the Pd precursor but another Pd species that interacted strongly with Cr.

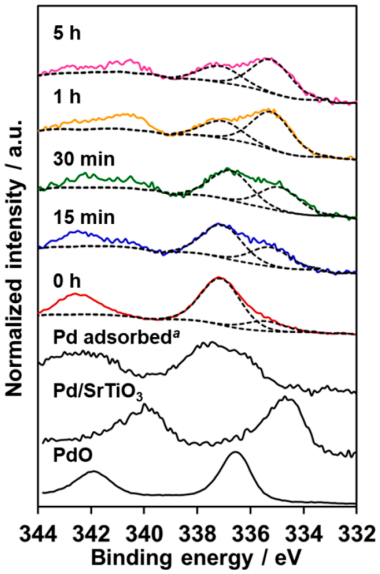

Figure 6. The XPS Pd 3d spectra for $PdCrO_x/SrTiO_3$ prepared at various time periods (0–5 h). Data for PdO and $Pd/SrTiO_3$ are shown as references. [a] Pd precursor ($Na_2PdCl_4 \cdot 3H_2O$) adsorbed on $SrTiO_3$ under dark conditions.

In the case of Cr, the Cr 2p peak in various $PdCrO_x/SrTiO_3$ samples was located in a position similar to Cr_2O_3, as shown in Figure S2. Therefore, the valence state of Cr on the surface of $PdCrO_x/SrTiO_3$ is independent of the photoirradiation conditions.

On the basis of the XAFS and XPS measurements, it is thus likely that the deposited core/shell nanostructures on $SrTiO_3$ consist of metallic Pd, oxidized Pd, and Cr^{III} (i.e., Cr_2O_3), where the core and shell are mainly formed by metallic Pd and Cr_2O_3, respectively, with oxidized Pd species being located at the core/shell interface. However, we could not observe the oxidized Pd species in the TEM images shown in Figure 3, due to the compositional inhomogeneity of the deposited nanoparticles.

2.5. Effect of $PdCrO_x$ Nanoparticles deposited on $SrTiO_3$ upon the Photocatalytic Activity toward Overall Water Splitting

The as-prepared $PdCrO_x/SrTiO_3$ samples were used to conduct photocatalytic reactions. Table 1 shows the overall water-splitting activities of $PdCrO_x/SrTiO_3$ prepared for various time periods (0–5 h). The 0 h sample produced H_2 and O_2; however, the H_2/O_2 ratio was not stoichiometric (entry 1). The total amount of H_2 and O_2 was increased, and the stoichiometry was improved with an increase of the irradiation time (entries 2–5). Therefore, longer irradiation times were effective to maximize the promotional effect of $PdCrO_x$ nanoparticles on photocatalytic water splitting.

Table 1. Photocatalytic overall water-splitting activities of $PdCrO_x/SrTiO_3$ prepared for various time periods (0–5 h)[a].

Entry	Sample	Loaded Cr/wt%	Rate of Gas Evolution/μmol h^{-1}	
			H_2	O_2
1	0 h	0.2	6.4	0.2
2	15 min	0.6	6.5	1.9
3	30 min	0.6	9.4	4.3
4	1 h	0.7	14.7	4.7
5	5 h	0.8	14.0	5.7
6	$SrTiO_3$	-	0.1	N. D.
7	$Pd/SrTiO_3$	-	3.4	0.3
8	$Cr_2O_3/Pd/SrTiO_3$	0.5	5.3	1.7

[a] Reaction conditions: Catalyst, 100 mg; pure water, 140 mL; metal precursors, Pd 0.5 wt%, Cr 1.0 wt%; light source, 300 W xenon lamp ($\lambda > 300$ nm).

Bare and only Pd-loaded $SrTiO_3$ were also used for comparison. Only H_2 was evolved at a very slow rate with the unmodified $SrTiO_3$ (entry 6); therefore, cocatalyst loading was necessary for overall water splitting. Pd-loaded $SrTiO_3$ produced H_2 and O_2 upon UV irradiation, although the H_2/O_2 ratio was far from stoichiometric (entry 7). As reported previously, molecular O_2 present in the reaction system can prevent stoichiometric water splitting on a semiconductor photocatalyst, because it can cause backward reactions [16]. Therefore, a suitable modification method such as Cr_2O_3-shell modification [13,19] is essential to suppress O_2-related backward reactions and efficiently allow overall water splitting to proceed. Both the stoichiometry and the amount of evolved gases were improved by the loading of a thin Cr_2O_3 shell on the Pd particles (entry 8). However, the activity of the Pd-core/Cr_2O_3-shell system was much lower than that of the optimized $PdCrO_x/SrTiO_3$. This provides clear evidence of the superior functionality of the optimally-synthesized $PdCrO_x$ nanoparticles as cocatalysts. Our previous work has also shown that the photocatalytic activity of $PdCrO_x/SrTiO_3$ (equivalent to the present 5 h sample) for overall water splitting is recoverable, with negligible changes in the valence state of Pd and Cr [16].

In Cr-containing mixed metal (oxide) cocatalysts, the key factors to enhance the promotional effect on photocatalytic water splitting are improvement of the H_2 evolution activity and the suppression of backward reactions (including H_2/O_2 recombination and O_2 photoreduction) [14]. For example, Cr(III) oxide shells formed on noble metal nanoparticles (cores) prevents these backward reactions [19]. We have previously reported that $PdCrO_x$ nanoparticles with a similar core/shell type structure had the same functionality [17].

The promotional effect of $PdCrO_x$ nanoparticles on photocatalytic H_2 evolution was investigated using methanol as an electron donor. Note that, in this reaction, methanol is irreversibly oxidized, with no O_2 evolution [17]. As listed in Table 2, all of the tested samples produced H_2. The 15 min sample, which exhibited relatively low activity for overall water splitting (see Table 1), gave the highest activity among the tested samples (entry 2), although the difference in activity among the $PdCrO_x/SrTiO_3$ samples was not very large. The Pd metal and Pd/Cr_2O_3 (core/shell) type samples exhibited lower activity (entries 6 and 7). A Cr_2O_3 shell formed on the surface of noble metal nanoparticles has been reported to prevent not only back reaction but also proton reduction to produce H_2 to a certain extent [19]. The H_2 evolution activity using $Pd/SrTiO_3$ was decreased by the stepwise photodeposition of Cr_2O_3 thin shell, as shown in Figure S3. The H_2 evolution activity of $PdCrO_x/SrTiO_3$ should be reduced with an increase of the irradiation time due to an increase of the amount of loaded Cr, because the reaction sites are covered with the Cr_2O_3 shells. However, the observed H_2 evolution activities were not simply decreased by Cr co-loading, as evident in Table 2. Therefore, it is suggested that interaction between Pd and Cr enhanced the intrinsic H_2 evolution activity, although the mechanistic detail is still under investigation. Nevertheless, the H_2 evolution activity of $PdCrO_x$ is not significantly changed by the photoirradiation time. Therefore, it is

worth considering that there is another factor that influences the overall water-splitting activity of $PdCrO_x/SrTiO_3$.

Table 2. Photocatalytic hydrogen evolution activity using $PdCrO_x/SrTiO_3$ prepared for various time periods (0–5 h)[a].

Entry	Sample	Loaded Cr/wt%	Rate of H_2 Evolution/μmol h^{-1}
1	0 h	0.2	12.5
2	15 min	0.6	57.4
3	30 min	0.6	44.2
4	1 h	0.7	50.0
5	5 h	0.8	47.4
6	$Pd/SrTiO_3$	0	43.3
7	$Cr_2O_3/Pd/SrTiO_3$	0.5	28.2

[a] Reaction conditions: Catalyst, 100 mg; 10 vol% aqueous methanol solution, 140 mL; metal precursors, Pd 0.5 wt%, Cr 1.0 wt%; light source, 300 W xenon lamp (λ > 300 nm).

We also considered that backward reaction caused by evolved O_2 could influence the water-splitting activity. Therefore, two types of backward reaction (H_2/O_2 recombination and O_2 photoreduction) were examined. Table 3 compares the rates of H_2/O_2 recombination using the 15 min and 5 h samples, as well as Pd-loaded $SrTiO_3$. In contrast to $Pd/SrTiO_3$, which exhibited very fast H_2/O_2 recombination, the $PdCrO_x$ loaded samples exhibited much slower recombination rates.

Table 3. Recombination activity of H_2 and O_2 over $PdCrO_x/SrTiO_3$ (15 min, 5 h)[a].

Entry	Sample	Loaded Cr/wt%	Rate of Diminished Gases/μmol h^{-1}	
			H_2	O_2
1	15 min	0.6	0.1	trace
2	5 h	0.8	2.0	1.7
3	$Pd/SrTiO_3$	-	24.6	12.2

[a] Reaction conditions: Catalyst, 25 mg; 10 vol% aqueous methanol solution, 100 mL; metal precursors, Pd 0.5 wt%, Cr 1.0 wt%; dark conditions; initially contained gases, H_2 400 μmol and O_2 200 μmol.

Oxygen photoreduction activity was also investigated during photocatalytic H_2 evolution in the presence or absence of O_2. The introduction of O_2 had a negative impact on the H_2 evolution activity. As detailed in Table 4, almost 97% of the initial activity was lost in the 15 min sample. Nevertheless, the 5 h sample still maintained approximately 20% of the initial activity, even in the presence of O_2. The difference in the H_2 evolution activity between the two samples is in qualitative agreement with the difference in the O_2 consumption activity. It is thus clear that O_2 photoreduction occurred more actively on the 15 min sample than on the 5 h sample. Therefore, more effective suppression of O_2 photoreduction could be realized by longer time photoirradiation during the preparation of $PdCrO_x$.

Table 4. Rates of H_2 evolution and O_2 consumption over $PdCrO_x/SrTiO_3$ samples (15 min and 5 h) in the presence or absence of O_2[a].

Entry	Sample	Loaded Cr/wt%	Atmosphere	Rate/μmol h^{-1}	
				H_2 Evolution	O_2 Consumption
1	15 min	0.6	Ar	37.5	-
2	15 min	0.6	Ar + O_2	1.1	47.7
3	5 h	0.8	Ar	28.1	-
4	5 h	0.8	Ar + O_2	5.5	23.6

[a] Reaction conditions: Catalyst, 100 mg; 10 vol% aqueous methanol solution, 140 mL; metal precursors, Pd 0.5 wt%, Cr 1.0 wt%; light source, 300 W xenon lamp (λ > 300 nm); atmosphere condition, 3.8 kPa Ar or 1.9 kPa Ar + 1.9 kPa O_2.

3. Materials and Methods

3.1. Synthesis of $SrTiO_3$

The $SrTiO_3$ was prepared using the polymerized complex method [6]. Titanium tetraisopropoxide (95.0+%, FUJIFILM Wako Pure Chemical, Osaka, Japan) was dissolved in methanol. Anhydrous citric acid (FUJIFILM Wako Pure Chemical, Osaka, Japan) was then added to the solution and heated at 353 K. $SrCO_3$ (99.9%, Kanto Chemical, Tokyo, Japan) and ethylene glycol (>99.5%, FUJIFILM Wako Pure Chemical, Osaka, Japan) were added to the solution. After heating at 423 K overnight for polymerization to proceed, the solution was heated in air at 573 K, and then at 823 K for 2 h to remove organic residues. The precursor was finally calcined at 1423 K for 2 h.

3.2. Cocatalyst Loading

The $PdCrO_x$ cocatalyst was deposited on the surface of $SrTiO_3$ by a simultaneous photodeposition method, as reported previously [16]. An amount of 0.2 g of $SrTiO_3$ was dispersed in 100 mL of 10 vol% methanol aqueous solution containing 1.0 wt% Cr (vs. $SrTiO_3$) from K_2CrO_4 and 0.5 wt% Pd (vs. $SrTiO_3$) from $Na_2PdCl_4 \cdot 3H_2O$ (FUJIFILM Wako Pure Chemicals Co., Osaka, Japan) as precursors. The solution was completely degassed and irradiated at room temperature for various time periods of 0–5 h. Evolved gases were detected using gas chromatography (GC-3200, Shimadzu Co., Kyoto, Japan) with a thermal conductivity detector (TCD), an MS-5A column and argon as a carrier gas (GL Science Co., Tokyo, Japan).

The amount of K_2CrO_4 (i.e., deposited Cr) remaining in solution was quantified using UV-visible absorption spectroscopy. First, the $PdCrO_x/SrTiO_3$ powder was collected by filtration and dried overnight at 343 K. After the addition of 0.27 mmol of EDTA·2Na (99.5%, Dojin Chem., Tokyo, Japan) to the filtrate, the mixture was boiled for 0.5 h. The solution was analyzed using UV-visible absorption spectroscopy.

3.3. Characterization

Prepared samples were studied using TEM, XAFS and XPS. TEM observations and the combined EDX were conducted using a JEM-2010F apparatus (JEOL, Tokyo, Japan). The Pd and Cr K-edge XAFS spectra were collected at AR-NW10A of the Photon Factory Advanced Ring and BL-9A of the Photon Factory, respectively (Proposal no. 2014S2-006, Photon factory, Tsukuba, Japan). Standard samples (Pd foil, PdO, Cr foil, Cr_2O_3) were measured by the transmission method. PdO and Cr_2O_3 were diluted in boron nitride and compressed to form pellets. Various $PdCrO_x/SrTiO_3$ samples prepared for various photoirradiation times (0–5 h) were measured by the fluorescence method using a multichannel solid state detector. The photon energies were calibrated according to the X-ray absorption edge of Pd foil (24350 eV) and Cr foil (5989 eV). Analysis of the raw XAFS spectra was conducted using the Athena and Artemis programs [22]. The Fourier transforms of the k^3-weighted EXAFS spectra were typically in the 3.0–11 $Å^{-1}$ region. The XPS spectra were obtained using an ESCA 3400 (Shimadzu, Kyoto, Japan) with a Mg anode. The binding energy of the C 1s peak (285.0 eV) that originated from adventitious carbon was used as the XPS reference.

3.4. Photocatalytic Reaction

Water-splitting reactions were conducted in a top-irradiation cell connected to a closed gas circulation system. An amount of 0.1 g of $PdCrO_x/SrTiO_3$ was dispersed in 140 mL of distilled water or 10 vol% aqueous methanol solution. The reactant solutions were degassed completely, followed by photoirradiation (Xe lamp, 300 W, 20 A, $\lambda \geq 300$ nm). Evolved gases were analyzed using gas chromatography. The reproducibility of the gas evolution rate was within ~20%.

3.5. Backward Reactions

Water formation from H_2 and O_2 was conducted under similar conditions to that for the photocatalytic reaction. An amount of 0.025 g of $PdCrO_x/SrTiO_3$ was dispersed in pure water. The reactant solution and gas phase were degassed completely and purged with hydrogen and oxygen. The reduction of gases was observed under dark conditions. Photocatalytic O_2 reduction activity was investigated under similar experimental conditions to those used for the photocatalytic hydrogen evolution reaction with O_2.

4. Conclusions

Photochemical preparation of $PdCrO_x$ multi-component nanoparticles on $SrTiO_3$ was studied to develop a new cocatalyst for overall water splitting. The valence state and fine structure of the Pd species in $PdCrO_x$ were strongly dependent on the photoirradiation time during $PdCrO_x$ deposition. The Pd species in $PdCrO_x$ was changed from oxide to oxide/metal mixed phase with an increase of the photoirradiation time, which contributed to enhanced activity for overall water splitting. The results of photocatalytic reactions indicated that the effect of activity enhancement was due to the suppression of O_2-photoreduction, a backward reaction of overall water splitting.

Supplementary Materials: The following are available online at http://www.mdpi.com/2073-4344/9/1/59/s1: Figure S1: (**A**) XANES spectra and (**B**) Fourier transforms of k^3-weighted Cr K-edge of $PdCrO_x$ nanoparticles (0–5 h) on $SrTiO_3$; Figure S2: XPS Cr 2p spectra of $PdCrO_x/SrTiO_3$ prepared for various time periods (0–5 h). Data for K_2CrO_4 and Cr_2O_3 are shown as references; Figure S3: Time course of H_2 evolution over Pd or Cr_2O_3/Pd nanoparticle loaded $SrTiO_3$.

Author Contributions: T.K. conducted most of the experiments and analysis. T.K. and K.M. designed the experiments; T.K., S.N. and D.L. performed the experiments and analyzed the data; T.K. and K.M. wrote the manuscript. All authors discussed and provided comments on the experiments and the manuscript during preparation.

Funding: This work was also partially supported by a Grant-in-Aid for Scientific Research on Innovative Areas "Mixed Anion" (Project JP16H06441) and "I^4LEC" (Project JP17H06438) from the Japan Society for the Promotion of Science (JSPS). T.K. acknowledges financial support in the form of a JSPS Fellowship for Young Scientists (Project JP18J10548).

Acknowledgments: The authors thank Suzukakedai Materials Analysis Division, Technical Department, Tokyo Institute of Technology for the TEM measurements and Photon Factory, High Energy Accelerator Research Organization for the XAFS measurements.

Conflicts of Interest: The authors declare no conflicts of interest.

References

1. Maeda, K. Photocatalytic Water Splitting Using Semiconductor Particles: History and Recent Developments. *J. Photochem. Photobiol. C* **2011**, *12*, 237–268. [CrossRef]
2. Roger, I.; Shipman, A.M.; Symes, D.M. Earth-abundant catalysts for electrochemical and photoelectrochemical water splitting. *Nat. Rev. Chem.* **2017**, *1*, 0003. [CrossRef]
3. Yang, X.; Wang, D. Photocatalysis: From Fundamental Principles to Materials and Applications. *ACS Appl. Energy Mater.* **2018**, *1*, 6657–6693. [CrossRef]
4. Maeda, K.; Mallouk, E.T. Two-Dimensional Metal Oxide Nanosheets as Building Blocks for Artificial Photosynthetic Assemblies. *Bull. Chem. Soc. Jpn.* **2019**, *92*, 38–54. [CrossRef]
5. Ham, Y.; Hisatomi, T.; Goto, Y.; Moriya, Y.; Sakata, Y.; Yamakata, A.; Kubota, J.; Domen, K. Flux-mediated doping of $SrTiO_3$ photocatalysts for efficient overall water splitting. *J. Mater. Chem. A* **2016**, *4*, 3027–3033. [CrossRef]
6. Kato, H.; Kobayashi, M.; Hara, M.; Kakihana, M. Fabrication of $SrTiO_3$ exposing characteristic facets using molten salt flux and improvement of photocatalytic activity for water splitting. *Catal. Sci. Technol.* **2013**, *3*, 1733–1738. [CrossRef]
7. Kato, H.; Kudo, A. Visible-Light-Response and Photocatalytic Activities of TiO_2 and $SrTiO_3$ Photocatalysts Codoped with Antimony and Chromium. *J. Phys. Chem. B* **2002**, *106*, 5029–5034. [CrossRef]

8. Kasahara, A.; Nukumizu, K.; Hitoki, G.; Takata, T.; Kondo, J.N.; Hara, M.; Kobayashi, H.; Domen, K. Photoreactions on $LaTiO_2N$ under visible light irradiation. *J. Phys. Chem. A* **2002**, *106*, 6750–6753. [CrossRef]
9. Maeda, K.; Teramura, K.; Lu, D.; Takata, T.; Saito, N.; Inoue, Y.; Domen, K. Photocatalyst releasing hydrogen from water. *Nature* **2006**, *440*, 295. [CrossRef]
10. Kuriki, R.; Ichibha, T.; Hongo, K.; Lu, D.; Maezono, R.; Kageyama, H.; Ishitani, O.; Oka, K.; Maeda, K. A Stable, Narrow-Gap Oxyfluoride Photocatalyst for Visible-Light Hydrogen Evolution and Carbon Dioxide Reduction. *J. Am. Chem. Soc.* **2018**, *140*, 6648–6655. [CrossRef]
11. Domen, K.; Kudo, A.; Onishi, T. Mechanism of photocatalytic decomposition of water into H_2 and O_2 over NiO-$SrTiO_3$. *J. Catal.* **1986**, *102*, 92–98. [CrossRef]
12. Maeda, K.; Teramura, K.; Saito, N.; Inoue, Y.; Domen, K. Improvement of photocatalytic activity of $(Ga_{1-x}Zn_x)(N_{1-x}O_x)$ solid solution for overall water splitting by co-loading Cr and another transition metal. *J. Catal.* **2006**, *243*, 303–308. [CrossRef]
13. Maeda, K.; Teramura, K.; Lu, D.; Saito, N.; Inoue, Y.; Domen, K. Noble-Metal/Cr_2O_3 Core/Shell Nanoparticles as a Cocatalyst for Photocatalytic Overall Water Splitting. *Angew. Chem. Int. Ed.* **2006**, *45*, 7806–7809. [CrossRef] [PubMed]
14. Maeda, K.; Teramura, K.; Masuda, H.; Takata, T.; Saito, N.; Inoue, Y.; Domen, K. Efficient Overall Water Splitting under Visible-Light Irradiation on $(Ga_{1-x}Zn_x)(N_{1-x}O_x)$ Dispersed with Rh-Cr Mixed-Oxide Nanoparticles: Effect of Reaction Conditions on Photocatalytic Activity. *J. Phys. Chem. B* **2006**, *110*, 13107–13112.
15. Maeda, K.; Lu, D.; Teramura, K.; Domen, K. Direct deposition of nanoparticulate rhodium–chromium mixed-oxides on a semiconductor powder by band-gap irradiation. *J. Mater. Chem.* **2008**, *18*, 3539–3542. [CrossRef]
16. Kanazawa, T.; Maeda, K. Light-Induced Synthesis of Heterojunctioned Nanoparticles on a Semiconductor as Durable Cocatalysts for Hydrogen Evolution. *ACS Appl. Mater. Interfaces* **2016**, *8*, 7165–7172. [CrossRef] [PubMed]
17. Kanazawa, T.; Lu, D.; Maeda, K. Photochemical Synthesis of Fe(III)–Cr(III) Mixed Oxide Nanoparticles on Strontium Titanate Powder and Their Application as Water Oxidation Cocatalysts. *Chem. Lett.* **2016**, *45*, 967–969. [CrossRef]
18. Higashi, M.; Domen, K.; Abe, R. Fabrication of an Efficient $BaTaO_2N$ Photoanode Harvesting a Wide Range of Visible Light for Water Splitting. *J. Am. Chem. Soc.* **2013**, *135*, 10238–10241. [CrossRef]
19. Yoshida, M.; Takanabe, K.; Maeda, K.; Ishikawa, A.; Kubota, J.; Sakata, Y.; Ikezawa, Y.; Domen, K. Role and function of noble-metal/Cr-layer core/shell structure cocatalysts for photocatalytic overall water splitting studied by model electrodes. *J. Phys. Chem. C* **2009**, *113*, 10151–10157. [CrossRef]
20. Ohno, T.; Sarukawa, K.; Matsumura, M. Crystal faces of rutile and anatase TiO_2 particles and their roles in photocatalytic reactions. *New J. Chem.* **2002**, *26*, 1167–1170. [CrossRef]
21. Brun, M.; Berthet, A.; Bertolini, C.J. XPS, AES and Auger parameter of Pd and PdO. *J. Electron Spectrosc. Relat. Phenom.* **1999**, *104*, 55–60. [CrossRef]
22. Ravel, B.; Newville, M. ATHENA, ARTEMIS, HEPHAESTUS: data analysis for X-ray absorption spectroscopy using IFEFFIT. *J. Synchrotron Radiat.* **2005**, *12*, 537–541. [CrossRef] [PubMed]